On the role of Eurasian autumn snow cover in dynamical seasonal predictions

Published Version:
On the role of Eurasian autumn snow cover in dynamical seasonal predictions / Ruggieri P.; Benassi M.; Materia S.; Peano D.; Ardilouze C.; Batte L.; Gualdi S.. - In: CLIMATE DYNAMICS. - ISSN 0930-7575. - STAMPA. - 58:7-8(2022), pp. 2031-2045. [10.1007/s00382-021-06016-z]

Availability:
This version is available at: https://hdl.handle.net/11585/864508 since: 2023-03-22

Published:
DOI: http://doi.org/10.1007/s00382-021-06016-z

Noname manuscript No.
(will be inserted by the editor)

On the role of Eurasian autumn snow cover in dynamical seasonal predictions

Paolo Ruggieri, Marianna Benassi, Stefano Materia, Daniele Peano, Constantin Ardilouze, Lauriane Batté, Silvio Gualdi

Received: date / Accepted: date

Abstract Seasonal predictions leverage on predictable or persistent components of the Earth system that can modify the state of the atmosphere. The land surface provides predictability through various mechanisms, including snow cover, with particular reference to Autumn snow cover over the Eurasian continent. The snow cover alters the energy exchange between surface and atmosphere and induces a diabatic cooling that in turn can affect the atmosphere locally and remotely. Lagged relationships between snow cover in Eurasia and atmospheric modes of variability in the Northern Hemisphere have been documented but are deemed to be non-stationary and climate models typically do not reproduce observed relationships with consensus. The role of the snow in recent dynamical seasonal forecasts is therefore unclear. Here we assess the role of Autumn Eurasian snow cover in a set of 5 operational seasonal forecasts with large ensemble size and high resolution and with the help of targeted idealised simulations. Forecast systems reproduce realistically regional changes of the surface energy balance. Retrospective forecasts and idealised sensitivity experiments identify a coherent change of the circulation in the Northern Hemisphere. The main features of the atmospheric response are a wave-train downstream over the Pacific and North America and a signal in the Arctic. The latter does not emerge in reanalysis data but is compatible with a lagged but weak and fast feedback from the snow to the Arctic Oscillation.

Keywords Seasonal climate predictions · Eurasian Snow Cover

F. Author
Department of Physics and Astronomy,
University of Bologna, Via Irnerio, 46, 40122, Bologna Italy and Fondazione CMCC, Bologna, Italy E-mail: paolo.ruggieri2@unibo.com

Marianna Benassi, Daniele Peano, Stefano Materia
Fondazione CMCC, Bologna, Italy,

Constantin Ardilouze, Lauriane Batté
CNRM, Météo-France, CNRS

Silvio Gualdi
Fondazione CMCC, Bologna and Istituto Nazionale di Geofisica e Vulcanologia, Bologna

1 Introduction

The role of autumn Eurasian snow cover for the interannual variability of the Northern Hemisphere climate was examined by many studies. Observational evidence promoted the concept of a causal relationship between snow cover and the Northern Hemisphere annular mode. This linkage is also exemplified by the relationship between snow cover and the near-surface Arctic Oscillation (AO) or the North Atlantic Oscillation [NAO, Saito and Cohen, 2003, Garfinkel et al., 2020]. The AO/NAO are dominant modes of variability for the circulation of, respectively, the Northern Hemisphere and the north Atlantic. Emphasis has been posed on a stratospheric pathway [Cohen et al., 2014a, 2007] that can be explained in terms of a coupled troposphere-stratosphere adjustment to surface forcing [Reichler et al., 2005, Fletcher et al., 2007]. This mechanism has implications for predictability on subseasonal and seasonal time scales, as it implies that autumn snow cover induces circulation changes in late autumn and in winter.
Years of development led to established empirical forecasts of either the AO or the NAO that are based also on indices of snow cover variability or support indirectly the role of the snow [e.g. Wang et al., 2017, Cohen and Jones, 2011]. More recently, snow cover has been successfully exploited in the implementation of a hybrid statistical-dynamical forecast of the NAO via a redefinition (subsampling) of the ensemble that involves the state of snow cover [Dobrynin et al., 2018]. A number of studies demonstrated a snow-AO mechanism in idealised simulations [e.g. Smith et al., 2010, Fletcher et al., 2009, Orsolini and Kvamstø, 2009]. These studies find an impact of the snow cover on the circulation over the Pacific and North America that leads to enhanced wave propagation into the stratosphere. Nonetheless, Hardiman et al. [2008] showed that CMIP3 climate models do not reproduce the observed snow-stratosphere linkage and therefore fail to reproduce the impact on the AO/NAO. More recently, Gastineau et al. [2017] identified a snow-AO relationship in a small subset of CMIP5 models and called for targeted experiments to assess the causal relationship. Furtado et al. [2015] also confirmed that the relationship is not robust in CMIP5 models but emerges in some time intervals, indicating a non-stationarity of the process, and revealed a common bias in the modelled snow variability. Along these lines, recent studies [Peings et al., 2013, Douville et al., 2017] highlighted the non-stationarity of the observed snow-AO relationship in past decades. Li et al. [2019] examined the role of snow initialisation in a seasonal forecast system and suggested a compromise of a weak feedback of the snow onto the AO/NAO [see also Orsolini et al., 2016, Garfinkel et al., 2020]. Non-stationarity and model dependence of the snow-AO relationship pose questions on the role of snow in modern dynamical seasonal forecasts and the lack of a multi-model assessment in an operational context is potentially a gap in our view of the linkage. In this study we investigate the relationship between Eurasian snow cover variability in a set of state-of-art operational forecast systems. As discussed in section 2, by using the Copernicus Climate Change Service (C3S) retrospective forecasts, we can take advantage of large ensembles and high resolution models. We demonstrate consensus and realism in how models reproduce the modulation of the surface energy balance by snow cover variability. As the hindcast time series is short and the sampling of the state of the climate system is poor, signals in the atmosphere can be explained by a forcing other than the snow or more generally by a predictable component of the system. One example is variability of sea ice in

the Eurasian sector of the Arctic, which is known to be covariant with Eurasian snow [Cohen et al., 2014b, Gastineau et al., 2017] and has been linked with circulation changes in polar and subpolar regions [Ruggieri et al., 2016] on seasonal time scales. Similarly, the winter circulation in the Northern Hemisphere can be affected by a range of phenomena. Noticeable examples are El Nino Southern Oscillation and the Pacific-Decadal Oscillation [Benassi et al., 2021, Rao et al., 2019], the Quasi-Biennial Oscillation [Rao et al., 2020], the Madden-Julian Oscillation [Wang et al., 2020], the Atlantic Multidecadal Variability [Ruggieri et al., 2021, Ruprich-Robert et al., 2017]. To account for the shortness of the hindcast period and corroborate the attribution of the remote atmospheric adjustment, idealised simulations with prescribed snow cover are performed. The synthesis of this combined approach allows to identify robust features of the atmospheric response to snow cover and disclose potential applications. Results are presented in section 3 and discussed in section 4.

2 Methodology

2.1 Reanalysis, seasonal forecast and idealised simulations

The ERA5 [Hersbach et al., 2020] and ERA5-Land [Muñoz-Sabater et al., 2021] reanalyses of the European Centre for Medium-Range Weather Forecast are used in this study to obtain an estimate of the state of the surface energy balance and of the atmospheric circulation associated with Eurasian snow cover variability. Data used include snow cover, two-metre temperature, sea level pressure, geopotential height, surface thermal and shortwave net radiation, surface latent and sensible heat flux. Data are obtained on a monthly basis from the Copernicus Data Store on the native grid. Results presented in the study also include the analysis of retrospective forecasts performed with 5 operational forecast systems contributing to the Copernicus Climate Change Service (C3S). The retrospective forecasts or hindcasts cover the period from 1993 to 2016 and we use the nominal start date of October 1st. Models used are summarised in table 1 and details on model features and initialisation techniques are available through the C3S documentation (https://confluence.ecmwf.int/display/CKB/C3S+Seasonal+Forecasts). A qualitative description of the snow cover initialisation technique is given in table 1. Some models are initialised via a reanalysis field, other via a forced run, one indirectly via a coupled run with assimilation in the atmosphere. One advantage of these forecast systems is the relatively high number of ensemble members that allows to identify small signals. A drawback of the approach is that the time series is short, a fact that undermines a clean attribution of the signal to snow cover variability. To corroborate findings obtained with seasonal forecast and to facilitate the attribution of atmospheric signals to snow cover related surface forcing, we use idealized simulations with atmospheric general circulation models (AGCMs) performed within the MEDSCOPE project (https://www.medscope-project.eu/). Models used are the atmospheric component of CMCC-SPS3 [Sanna et al., 2016, , one of the models contributing to the C3S forecast] hereafter referred to as CMCC-AGCM, and the ARPEGE-Climat 6.3 [Roehrig et al., 2020] hereafter referred to as MF-AGCM. A reference control (hereafter CONTROL) simulation and a forced experiment (hereafter SNOW), designed to mimic a snow cover increase in Eurasia (i.e. 42.5 to 72.5 °N, 40 to 180°E), have been performed. CONTROL is a 50-year integration with climatological monthly SSTs [computed over the period 1981-2010 from the HadiSST ocean analysis, Rayner et al., 2003] and using perpetual radiative forcing at year 2000 (i.e. present-day conditions), after spinup. On the other hand, SNOW is a 50-member ensemble of 6-month long integrations from the 1st of October with initial conditions taken from CONTROL. To prescribe an arbitrary snow cover field, the models land surface schemes have been modified to inhibit the interactive snow formation, accumulation, and melt over the region of interest. The methodology adapts the approach applied by Hauser et al. [2017] on soil moisture to snow water equivalent. With this method we restore the snow cover to a stationary state for the first two months of integration, while from December this constraint is not further applied and the system is free to evolve. The snow water equivalent values are prescribed to the average November snow water equivalent computed over the upper 25th percentile of the observed distribution in the 1913-2012 period from the NOAA-20CR reanalysis [as in Douville et al., 2017]. The quality of snow cover data in this reanalysis is also discussed in Douville et al. [2017]. As shown in the Results section, this definition imposes a forcing that mimics observed features of snow cover variability.

2.2 Methods

To quantify the variability of snow cover in Eurasia we introduce the Eurasian Snow Cover (ESC) index adapted from Douville et al. [2017]. Compared to Douville et al. [2017], we apply a small adjustment to the latitudinal boundaries to facilitate the implementation of a snow cover restoring in idealised simulations. The ESC index is defined as the area-weighted average of the snow cover area fraction (snow cover) of ERA5-Land in the domain 40-180°E, 42.5-72.5°N in October. This index is therefore proportional to the fraction of the domain covered by snow. Note that in the reanalysis the snow cover is diagnosed from other prognostic variables. The choice of the the snow cover over other snow-related variables is guided by its established impact with the near-surface climate and is common to previous studies [e.g. Douville et al., 2017, Gastineau et al., 2017]. For models, linear regressions are computed using the ESC index of the reanalysis as predictor and the ensemble mean of a modelled quantity as predictand. Statistical significance for regressions has been computed using the Wald test [Wald and Wolfowitz, 1940] to reject the null hypothesis that the slope is zero. The atmospheric response to snow forcing in idealised experiments is defined as the difference between the ensemble mean of SNOW and the ensemble mean of CONTROL. Statistical significance for idealised experiments is assessed using a t-test to reject the null hypothesis that the means belong to the same distribution. The AO pattern is obtained as the first empirical orthogonal function of monthly sea level pressure, computed separately for each month. The strength of the stratospheric polar vortex is diagnosed with the average of the zonal mean zonal wind at 10 hPa in the band 50-65 °N [see e.g. Palmeiro et al., 2015].

3 Results

This section is divided into three parts. The first one where the relationship between snow cover, the local surface energy balance and the circulation in seasons ahead is investigated using a reanalysis. In the second one, linear regressions based on seasonal hindcasts are analysed to identify a predictable component of the atmospheric response to snow cover variability. In the third and final one, results presented in previous sections 3.1 and 3.2 are discussed in view of a set of idealised sensitivity model simulations in which snow cover is increased in Eurasia.

3.1 Snow cover variability and teleconnection in the reanalysis

The time series of the ESC index in the period covered by C3S hindcasts is shown in Fig. 1 by a solid black line. We note a peak around year 2000 followed by a drop between 2003 and 2012 and a second peak at the end of the time series. This behaviour is broadly in agreement with satellite-derived estimates of snow cover [not shown, Estilow et al., 2015]. The role of snow cover in the surface energy balance was examined by Cohen and Rind [1991] and the impact of the snow cover variability on surface energy fluxes is demonstrated by Fletcher et al. [2009, see their figure 1]. The presence of snow increases the reflected amount of shortwave radiation by increasing the surface albedo and cools the surface. A cooler surface leads to reduced thermal and turbulent heat fluxes. Overall the combined effect of these changes cools the atmosphere and reduces the near surface air temperature. We see in Fig. 1 that the ESC index explains a large fraction of surface flux variability in its domain, with the correlation between ESC and the net shortwave flux reaching 0.75 (for the other components it is about -0.66). Note that in Fig. 1 the sign of the sum of thermal radiation and turbulent heat flux has been reversed to facilitate the comparison with the other time series. The correlation between the ESC index and grid point values of snow cover is shown in Fig. 2. It can be seen that the variability in the period 1993-2016 described by the ESC index is mostly representative of the western part of the sector, although positive correlations are found over more than 90% of the land grid points in the domain. Fig. 2 also suggests that October snow cover anomalies persist in November in some regions, and up to winter in the Ural region. We conclude that the ESC index is associated with regional snow cover variability in a vast portion of Eurasia and is closely representative of snow cover variability in the Ural-Western-Siberia region. We examine hereafter the surface energy balance and to account for the persistence of the snow cover anomalies (Fig. 2) we look at October-November bimonthly averages.

The relationship between the ESC index and the local surface energy balance in the reanalysis is examined in Fig. 3. Grey rectangles encompass the area used to compute averaged quantities displayed in Fig. 1. We can identify three regions where a considerable fraction of the variability of surface fluxes is explained by the ESC index: in the Ural region, in Eastern Siberia and in Western Siberia. In these regions, correlations reach about ± 0.75 and a linear regression suggests that the ESC index can explain up to about 10 $\mathrm{Wm^{-2}}$.

The surface shortwave flux is positively correlated also in smaller scale regions in East Asia and a negative correlation is found in a small area to the south and to the east of the Central Siberian Plateau. The negative correlation can be interpreted in terms of a weaker snow cover variability in this region. The sum of other components of the energy flux (Fig. 3,c) confirms the regional signature of snow cover variability found in Fig. 3,a. These findings hold for the individual addenda of Fig. 3,c (not shown). Such alteration of the surface energy balance leads to a cooler atmosphere, as confirmed by Fig. 3,d, where we see that negative correlations with near-surface air temperature cover most of the domain. The snow cover variability captured by the ESC index can modulate the near surface air temperature in Eurasia by 4 K, presumably with a stronger impact on the western part of the domain, where also changes in surface fluxes are stronger. A fraction of the temperature signal is likely explained by the atmospheric circulation in October (Fig. 4,a), that features a barotropic low over western Siberia and the northerly flow over the Ural region, coincident with the most negative correlation in Fig. 3,d. A similar pattern, prior to episodes of snow cover increase in western Siberia on an intraseasonal time scale, is discussed by Song and Wu [2019]. Moreover, we see a barotropic high in the Arctic, from the Barents to the Laptev sea, and a surface high in Eastern Siberia, both are statistically significant at the chosen confidence level and the latter is likely explained by a shallow thermodynamic adjustment to local snow cover increase, perhaps in phase with an independent surface high. With the same rationale, the low over Siberia could be masking the snow feedback on sea level pressure. These statements are discussed more in details in section 3.3. In November (not shown) a signal is found in the extratropical Pacific with a deep low covering most of the Northern part of the ocean and high located to the North. A shallow high over Barents sea and Urals is also found and the barotropic signal in the Pacific is persistent up to December and is detectable in seasonal average of NDJ (Fig. 4,b). The lack of a negative AO response in winter is noticeable and is common also to late winter (Fig. 4,c and d). The picture given by Fig. 4 is likely to be contaminated by atmospheric noise that is unrelated to nor induced by snow cover or any deterministic surface forcing. Ensembles of dynamical seasonal forecast can help us detect a predictable component of the feedback of the snow onto the atmosphere and they are analysed in section 3.2.

3.2 Eurasian snow cover in recent seasonal forecasts

Results presented in this section are based on regressions onto the ERA5-Land ESC index of atmospheric and surface variables in a multi-model ensemble of seasonal forecasts. The regressions is computed for ensemble mean quantities of each model separately, over the period (1993-2016). Models used are described in section 2.1 and in table 1. In Figs. 5 and 6 we can see that all models simulate the observed modulation of the surface energy balance by snow cover and they reproduce regional features with good accuracy. In seasonal hindcasts, as for ERA5, the surface forcing to the atmosphere associated with snow cover variability is particularly strong in the Ural-Western-Siberia region. This analysis shows that the current generation of dynamical seasonal forecasts reproduces the signature of snow cover variability on a regional scale. We can therefore investigate the dependence of the forecast of the tropospheric circulation on the snow cover extent in Eurasia. In Fig. 7 we see the multi-model mean of the regression of Z500 and SLP, i.e. the mean of the 5 regression coefficients computed for each model alone.

We can see that in regions where a signal emerges all models agree on the sign of the regression (stippled regions). This result indicates that models agree on simulating a linear dependence of the forecast on the Eurasian snow cover variability captured by the ESC index. It also reassures that signals in the multimodel mean are not dominated by one or some of the models of the ensemble. It can be seen that, in October (Fig. 7,a), all models show a wave-train from the North Atlantic which at 500 hPa peaks with a low over Siberia, where there is no signal in the sea level pressure. The surface pressure peaks instead in the Barents sea and in Scandinavia. The Scandinavian pattern and the low over western Siberia are precursors of snow cover increase in the region [Gastineau et al., 2017, Song and Wu, 2019], but a similar pattern emerges also in response to snow cover increase, as shown later, and it is found in the reanalysis (Fig. 4). This configuration can be interpreted assuming that the models predict the linear, local response over Eurasia plus a predictable signal confined in the first weeks. The statement on the linear response is confirmed by results presented in section 3.3. After the first month, seasonal averages are dominated by the negative barotropic anomaly in the Pacific and the positive one further downstream over the American continent. A shallow high from the Barents to the Laptev sea develops throughout the seasons, deepens and enlarges into the Labrador sea.
While the snow can be linked with the local adjustment of the pressure and of the geopotential, the robust remote response in the Arctic and in the Pacific can be explained also by a different forcing. Large ensembles of seasonal forecasts are indeed a valuable tool to identify the predictable signal even if the magnitude of the signal is small compared to that of the noise, but are so far available for a relatively short period. The shortness of the time series introduces a major limitation on the attribution of the signal. To mitigate this issue a set of idealised simulations has been performed and results based on these idealised simulations are presented in the following section.

3.3 Idealised simulations

Idealised simulations with two AGCMs have been performed to corroborate findings obtained with the seasonal forecasts. The setup is such that the control simulation performed with climatological sea ice and SSTs and freely evolving snow cover (CONTROL) is compared with a perturbed run where the snow extent in Eurasia is imposed to be substantially larger in October and November (SNOW). Both are 6-month ensemble simulations starting in October. Details on the setup and the models are given in section 2.1. The analysis is based on differences between the ensemble mean of the SNOW run minus that of the CONTROL run.
It can be seen from Fig. 8 that this idealised setup implies increased snow cover in the southern and in the western part of the domain and this is a desired feature of the surface forcing, in view of the results presented in Figs. 2, 4 and 5. However, the forcing is particularly strong in the southern boundary of the domain and covers also east Asia, which does not resemble closely the observed variability in the hindcast period. The intensity of the forcing decreases substantially between October and November especially for the CMCC model and a residual anomalous snow cover in the western part of the domain persists into winter, up to January (not shown). Overall this behaviour agrees qualitatively with the reanalysis. The

total snow cover extent of the domain in October is however exaggerated if compared to the interannual variability of seasonal forecasts used in this study. Surface fluxes (Fig. 9) are perturbed by the increased snow in a way that resembles what found in sections 3.1 and 3.2 in reanalysis and seasonal forecasts. The associated spatial patterns are not shown as they follow the pattern of snow cover change. We note the positive heat flux anomaly in the western Pacific, that can be explained in terms of a stronger heating by the ocean due to a colder overlaying atmosphere, which in turn is explained by advection by the predominantly westerly wind of air that is cooled by the presence of the snow. The abrupt fluctuation between 40 and 60 °E is explained by the intensified heat transfer from water to air in the Caspian sea.

To condense and compare results obtained by the two idealised simulations, in Fig. 10 we show atmospheric fields averaged in the midlatitudes, precisely between 42.5 °N and 72.5 °N, which is the latitudinal extent of the domain used to impose the snow cover perturbation and used in Fig. 3. As in forecast and reanalysis, the surface cooling is stronger in the western part of the domain, by construction in this case, and differences between the two models can be explained by differences in the surface flux change that in turn is proportional to a different snow cover anomaly. The temperature change is found in the boundary layer and in the free troposphere above and it persists but substantially decays in November.

The equivalent analysis for the circulation is rather interesting. In Fig. 10,c the dominant feature is a strongly baroclinic response that can be understood in the framework of a steady, linear adjustment a la Hoskins and Karoly [1981]. Both models reproduce a shallow high to the east of the cooling, advection of warm air from lower latitudes in the region of strong cooling (50-90 °E) and the vorticity anomaly increasing with height as implied by the negative Z500 signal. This regime of the response has been described for surface heating/cooling associated with high-latitude SST and sea ice variability [Deser et al., 2010, Ruggieri et al., 2017]. These studies found that the linear response is established within 1-2 days and dominates the anomalous circulation up to two-three weeks. After that, a response projecting onto a dominant mode of variability (AO-NAO) emerges. In our case, the linear response indeed dominates in the first month and is confined in the first 3 weeks of simulation (not shown). After one month, in November, albeit a persistent, residual forcing, there is no evidence of a surface cooling out of the boundary layer and of any signal attributable to the linear response. On the other hand, the two models show a coherent signal in the Pacific and in North America, broadly (but not exactly) coincident with a weakened Aleutian low. These findings highlight the emergence of a lagged and remote response that is arguably crucial for the predictability in the seasonal range.

The comparison between idealised experiments and seasonal forecasts is indeed particularly insightful. Fig. 11 shows a 1-2 month lagged atmospheric response to snow cover increase deduced with two different methods. In panel a), it is assessed using the multi-model (C3S) regression on the ESC index based on ERA5-Land. In panel b), it is assessed through the two-model ensemble mean difference in the idealised sensitivity experiments. Substantial and intriguing similarities can be noted, primarily in the Pacific-American sector. There is a wave-train peaking with a negative anomaly in the Eastern Pacific. In the Arctic, a rather shallow signal in the Kara and Laptev seas is found. On a finer scale, there are important differences: both are compatible with a local linear response to cooling at the surface in Eurasia, but this signature is remarkably stronger in the idealised experiments. This is expected and consistent with a stronger surface forcing. Finally over the North Atlantic and Europe, here it appears that uncertainty is larger, compared to other regions. Both approaches feature a low over the subpolar-gyre/Nordic-Seas and high over central and western Mediterranean. However the anomalous circulation is substantially different in the Euro-Atlantic. Perhaps this region is more sensitive to small differences in surface forcing, but in any case this sensitivity foresees large intrinsic uncertainty. Robust features in the Arctic and in the Pacific are confirmed by analysis of individual models. For instance, in Fig. 12, we can see the comparison of the regression with the CMCC forecast system and with the CMCC-AGCM, that is the atmospheric component of the forecast systems itself. The structure with a low over Siberia, a high over the Arctic and a low over the Eastern Pacific is confirmed. We also note that the CMCC and ECMWF forecast systems feature a stronger signal in the Pacific and in the Arctic compared to other models (not shown). This is in agreement with a stronger signal in the surface fluxes (Figs. 5 and 6). Fig. 12 also confirms a large uncertainty for the response in the Atlantic.

As discussed in the Introduction, previous studies have identified a stratospheric pathway for a delayed atmospheric response to snow cover. The timing of the robust features of the response can help understand whether the signal is related to a stratospheric pathway. The North Pacific response (Fig. 13a,b) is relatively fast, peaks in November and can be seen in bimonthly averages up to November-December, models agree on the timing of the signal. The shallow Arctic high (Fig. 13c,d) peaks later through the season and models slightly disagree on the timing with CMCC-AGCM showing the peak in December and MF-AGCM in January. Bimonthly averages show clearly that this signal persists into winter. In the stratosphere there is no evidence of any significant modification of the intensity of the polar vortex. We measure it with the average zonal mean zonal wind in the polar vortex edge (Fig. 13e,f, Palmeiro et al. [2015]). There is no evidence of a role for the stratosphere in the mechanism, but the tropospheric signal projects onto the model AO pattern (see table 2). Indeed, the peak of the signal in the Artic (Fig. 13c,d) is associated with a weak negative AO signal.

Forecasts and idealised simulations coherently suggest a potential for the predictability of temperature and precipitation over land driven by snow cover variability in some regions of Europe and North America. The latter can be seen in Fig. 14, where again forecast and idealised simulations provide a similar picture for the precipitation response over some areas of the extra-tropical North America. We note in particular sporadic signals of continental drying and a dipolar pattern of precipitation along the East coast of the continent. Nonetheless, there is little agreement with the corresponding regression with reanalysis. Differences with reanalysis (not shown) are attributable to a different tilt of the Pacific wave-train.

4 Concluding remarks

In this study retrospective seasonal forecasts with operational systems are combined with idealised simulations with state-of-the-art AGCMs to assess the atmospheric response to Eurasian snow cover variability in recent decades (1993-2016). Seasonal hindcasts reproduce regional features of Eurasian snow cover variability and the associated change in the surface energy balance. Reanalysis, seasonal forecasts and idealised experiments converge in indicating that an anomalous circulation in the Pacific is established after the first month and persists for about two months (Figs. 4, 7, 11, 13). Forecasts identify a robust relationship between snow cover and atmospheric circulation that can be attributed to snow cover variability by AGCM idealised simulations (Fig. 11). The modelled response projects onto the annular mode of variability of the model, but notably there is no evidence of changes in the stratospheric circulation (Fig. 13).

The geographical position of the surface forcing determines how the atmospheric flow responds. For the case of the snow, this can be understood primarily in terms of a linear interference between anomalous and climatological waves [Smith et al., 2010], but in also in view of how synoptic eddies respond [Ruggieri et al., 2019]. For the period considered in our study, autumn snow cover variability in Eurasia is dominated by western Siberia, but this does not generally apply to the twentieth century [Brown, 2000]. It follows that the lack of a stratospheric response could be linked with this specific feature of the forcing (e.g. whether it is stronger in western or eastern Siberia). On the other hand, part of the uncertainty of the response could be mitigated if we were able to sample the role of regional snow cover variability in sub-domains of Eurasia. In this sense, it could be that operational forecasts draw predictability from snow cover well beyond the picture given by Fig. 11. An interesting question is whether the snow-cover forcing closer to winter shows an impact on the polar vortex. Portal et al. [2021] showed that November start dates of the same seasonal forecasts used in this study are able to simulate realistically the variability of the polar vortex, the upward wave propagation and their relationship. It is therefore unlikely that the lack of the stratospheric pathway in this study is explained by model biases in the troposphere-stratosphere interaction. Portal et al. [2021] also find a weak and model dependent relationship between snow cover variability and the intensity of the polar vortex in the examined period for the November start date, that is consistent with results of Garfinkel et al. [2020] and Orsolini et al. [2016]. It is therefore plausible that start dates closer to winter may reveal a different picture.

Some inconsistencies between models are found in regional features of the surface flux variability associated with snow variability (Fig. 6). This can be partly explained by differences in the snow initialisation techniques. The use of reanalysis initialization for land surface could generate inconsistencies, resulting in a degradation of the forecast quality [Materia et al., 2014]. Improvements in the land initialisation and in land-atmosphere coupled data assimilation may reduce the model uncertainty for the atmospheric response to Eurasian snow cover variability and the value of development in this direction is advocated by our analysis. We find regional impacts in other regions, one example is the western Mediterranean where models show a surface high (Fig. 11) and reduced precipitation (not shown). But as this signal comes with a model dependent large scale response in Europe, associated impacts should be mentioned with caution. The substantial agreement between forecast, idealised simulations and to some extent reanalysis gives a clear picture of the atmospheric response to snow cover variability for many regions but the North Atlantic. This is arguably closely linked with the lack of role for the stratosphere, which also limits the lead time of the predictable component of the response to 2-3 months after initialisation. It is likely that persistence and prediction of snow cover anomalies will be crucial for practical purposes. In terms of the

Arctic Oscillation, our study indicates a weak but robust tropospheric feedback from the snow to the AO.

Acknowledgements The authors are thankful to three anonymous reviewers for their valuable comments. This study has been supported by the MEDSCOPE (MEDiterranean Services Chain based On climate PrEdictions) ERA4CS project (grant agree-ment no. 690462) funded by the European Union.

References

M. Benassi, G. Conti, S. Gualdi, P. Ruggieri, S. Materia, J. García-Serrano, F. M. Palmeiro, L. Batté, and C. Ardilouze. El niño teleconnection to the euro-mediterranean late-winter: the role of extratropical pacific modulation. *Climate Dynamics*, pages 1–21, 2021.

V. Brovkin, T. Raddatz, C. H. Reick, M. Claussen, and V. Gayler. Global biogeophysical interactions between forest and climate. *Geophysical Research Letters*, 36(7), 2009. doi: https://doi.org/10.1029/2009GL037543.

R. D. Brown. Northern Hemisphere Snow Cover Variability and Change, 1915–97. *Journal of Climate*, 13(13):2339–2355, 07 2000. ISSN 0894-8755. doi: 10.1175/1520-0442(2000)013¡2339:NHSCVA¿2.0.CO;2.

J. Cohen and J. Jones. A new index for more accurate winter predictions. *Geophysical Research Letters*, 38(21), 2011. doi: https://doi.org/10.1029/2011GL049626.

J. Cohen and D. Rind. The effect of snow cover on the climate. *Journal of Climate*, 4(7):689–706, 1991.

J. Cohen, M. Barlow, P. J. Kushner, and K. Saito. Stratosphere–troposphere coupling and links with eurasian land surface variability. *Journal of Climate*, 20 (21):5335–5343, 2007. doi: 10.1175/2007JCLI1725.1.

J. Cohen, J. C. Furtado, J. Jones, M. Barlow, D. Whittleston, and D. Entekhabi. Linking siberian snow cover to precursors of stratospheric variability. *Journal of Climate*, 27(14):5422–5432, 2014a.

J. Cohen, J. A. Screen, J. C. Furtado, M. Barlow, D. Whittleston, D. Coumou, J. Francis, K. Dethloff, D. Entekhabi, J. Overland, and J. Jones. Recent arctic amplification and extreme mid-latitude weather. *Nature Geosci*, 7(9):627–637, 09 2014b.

D. P. Dee, S. M. Uppala, A. J. Simmons, P. Berrisford, P. Poli, S. Kobayashi, U. Andrae, M. A. Balmaseda, G. Balsamo, P. Bauer, P. Bechtold, A. C. M. Beljaars, L. van de Berg, J. Bidlot, N. Bormann, C. Delsol, R. Dragani, M. Fuentes, A. J. Geer, L. Haimberger, S. B. Healy, H. Hersbach, E. V. Hólm, L. Isaksen, P. Kållberg, M. Köhler, M. Matricardi, A. P. McNally, B. M. Monge-Sanz, J.-J. Morcrette, B.-K. Park, C. Peubey, P. de Rosnay, C. Tavolato, J.-N. Thépaut, and F. Vitart. The era-interim reanalysis: configuration and performance of the data assimilation system. *Quarterly Journal of the Royal Meteorological Society*, 137(656):553–597, 2011. ISSN 1477-870X. doi: 10.1002/qj.828. URL `http://dx.doi.org/10.1002/qj.828`.

C. Deser, R. Tomas, M. Alexander, and D. Lawrence. The seasonal atmospheric response to projected arctic sea ice loss in the late twenty-first century. *Journal of Climate*, 23(2):333–351, 2010. doi: 10.1175/2009JCLI3053.1. URL `http://dx.doi.org/10.1175/2009JCLI3053.1`.

M. Dobrynin, D. I. Domeisen, W. A. Müller, L. Bell, S. Brune, F. Bunzel, A. Düsterhus, K. Fröhlich, H. Pohlmann, and J. Baehr. Improved teleconnection-based dynamical seasonal predictions of boreal winter. *Geophysical Research Letters*, 45(8):3605–3614, 2018.

H. Douville, Y. Peings, and D. Saint-Martin. Snow-(n)ao relationship revisited over the whole twentieth century. *Geophysical Research Letters*, 44(1):569–577, 2017. doi: https://doi.org/10.1002/2016GL071584.

T. W. Estilow, A. H. Young, and D. A. Robinson. A long-term northern hemisphere snow cover extent data record for climate studies and monitoring. *Earth System Science Data*, 7(1):137, 2015.

C. G. Fletcher, P. J. Kushner, and J. Cohen. Stratospheric control of the extratropical circulation response to surface forcing. *Geophysical Research Letters*, 34 (21), 2007.

C. G. Fletcher, S. C. Hardiman, P. J. Kushner, and J. Cohen. The dynamical response to snow cover perturbations in a large ensemble of atmospheric gcm integrations. *Journal of Climate*, 22(5):1208–1222, 2009. doi: 10.1175/2008JCLI2505.1.

J. C. Furtado, J. L. Cohen, A. H. Butler, E. E. Riddle, and A. Kumar. Eurasian snow cover variability and links to winter climate in the cmip5 models. *Climate dynamics*, 45(9-10):2591–2605, 2015.

C. I. Garfinkel, C. Schwartz, I. P. White, and J. Rao. Predictability of the early winter arctic oscillation from autumn eurasian snowcover in subseasonal forecast models. *Climate Dynamics*, 55:961–974, 2020.

G. Gastineau, J. García-Serrano, and C. Frankignoul. The influence of autumnal eurasian snow cover on climate and its link with arctic sea ice cover. *Journal of Climate*, 30(19):7599–7619, 2017.

S. C. Hardiman, P. J. Kushner, and J. Cohen. Investigating the ability of general circulation models to capture the effects of eurasian snow cover on winter climate. *Journal of Geophysical Research: Atmospheres*, 113(D21), 2008. doi: https://doi.org/10.1029/2008JD010623.

M. Hauser, R. Orth, and S. I. Seneviratne. Investigating soil moisture–climate interactions with prescribed soil moisture experiments: an assessment with the community earth system model (version 1.2). *Geoscientific Model Development*, 10(4):1665–1677, 2017.

H. Hersbach, B. Bell, P. Berrisford, S. Hirahara, A. Horányi, J. Muñoz-Sabater, J. Nicolas, C. Peubey, R. Radu, D. Schepers, A. Simmons, C. Soci, S. Abdalla, X. Abellan, G. Balsamo, P. Bechtold, G. Biavati, J. Bidlot, M. Bonavita, G. De Chiara, P. Dahlgren, D. Dee, M. Diamantakis, R. Dragani, J. Flemming, R. Forbes, M. Fuentes, A. Geer, L. Haimberger, S. Healy, R. J. Hogan, E. Hólm, M. Janisková, S. Keeley, P. Laloyaux, P. Lopez, C. Lupu, G. Radnoti, P. de Rosnay, I. Rozum, F. Vamborg, S. Villaume, and J.-N. Thépaut. The era5 global reanalysis. *Quarterly Journal of the Royal Meteorological Society*, 146 (730):1999–2049, 2020. doi: https://doi.org/10.1002/qj.3803.

B. J. Hoskins and D. J. Karoly. The steady linear response of a spherical atmosphere to thermal and orographic forcing. *Journal of the Atmospheric Sciences*, 38(6):1179–1196, 1981. doi: 10.1175/1520-0469(1981)038¡1179:TSLROA¿2.0.CO;2. URL `http://dx.doi.org/10.1175/1520-0469(1981)038<1179:TSLROA>2.0.CO;2`.

S. J. Johnson, T. N. Stockdale, L. Ferranti, M. A. Balmaseda, F. Molteni, L. Magnusson, S. Tietsche, D. Decremer, A. Weisheimer, G. Balsamo, et al. Seas5: the new ecmwf seasonal forecast system. *Geoscientific Model Development*, 12(3): 1087–1117, 2019.

S. Kobayashi, Y. Ota, Y. Harada, A. Ebita, M. Moriya, H. Onoda, K. Onogi, H. Kamahori, C. Kobayashi, H. Endo, et al. The jra-55 reanalysis: General specifications and basic characteristics. *Journal of the Meteorological Society of Japan. Ser. II*, 93(1):5–48, 2015.

P. Le Moigne, A. Boone, J. Calvet, B. Decharme, S. Faroux, A. Gibelin, C. Lebeaupin, J. Mahfouf, E. Martin, V. Masson, et al. Surfex scientific documentation. *Note de centre (CNRM/GMME), Météo-France, Toulouse, France*, 2009.

F. Li, Y. Orsolini, N. Keenlyside, M.-L. Shen, F. Counillon, and Y. Wang. Impact of snow initialization in subseasonal-to-seasonal winter forecasts with the norwegian climate prediction model. *Journal of Geophysical Research: Atmospheres*, 124(17-18):10033–10048, 2019.

S. Materia, A. Borrelli, A. Bellucci, A. Alessandri, P. Di Pietro, P. Athanasiadis, A. Navarra, and S. Gualdi. Impact of atmosphere and land surface initial conditions on seasonal forecasts of global surface temperature. *Journal of Climate*, 27(24):9253–9271, 2014.

J. Muñoz-Sabater, E. Dutra, A. Agustí-Panareda, C. Albergel, G. Arduini, G. Balsamo, S. Boussetta, M. Choulga, S. Harrigan, H. Hersbach, et al. Era5-land: A state-of-the-art global reanalysis dataset for land applications. *Earth System Science Data Discussions*, pages 1–50, 2021.

K. Oleson, D. Lawrence, G. Bonan, B. Drewniak, M. Huang, C. Koven, S. Levis, F. Li, W. Riley, Z. Subin, et al. Technical description of version 4.5 of the community land model (clm), ncar technical note: Ncar/tn-503+ str. *National Center for Atmospheric Research (NCAR), Boulder, CO, USA, https://doi.org/10.5065/D6RR1W7M*, 2013.

Y. Orsolini, R. Senan, F. Vitart, G. Balsamo, A. Weisheimer, and F. Doblas-Reyes. Influence of the eurasian snow on the negative north atlantic oscillation in subseasonal forecasts of the cold winter 2009/2010. *Climate Dynamics*, 47 (3-4):1325–1334, 2016.

Y. J. Orsolini and N. G. Kvamstø. Role of eurasian snow cover in wintertime circulation: Decadal simulations forced with satellite observations. *Journal of Geophysical Research: Atmospheres*, 114(D19), 2009. doi: https://doi.org/10.1029/2009JD012253.

F. M. Palmeiro, D. Barriopedro, R. García-Herrera, and N. Calvo. Comparing sudden stratospheric warming definitions in reanalysis data. *Journal of climate*, 28(17):6823–6840, 2015.

Y. Peings, E. Brun, V. Mauvais, and H. Douville. How stationary is the relationship between siberian snow and arctic oscillation over the 20th century? *Geophysical Research Letters*, 40(1):183–188, 2013.

A. Portal, P. Ruggieri, F. M. Palmeiro, J. García-Serrano, D. I. Domeisen, and S. Gualdi. Seasonal prediction of the boreal winter stratosphere. *Climate Dynamics*, pages 1–22, 2021.

J. Rao, C. I. Garfinkel, and R. Ren. Modulation of the northern winter stratospheric el niño–southern oscillation teleconnection by the pdo. *Journal of Climate*, 32(18):5761–5783, 2019.

J. Rao, C. I. Garfinkel, and I. P. White. How does the quasi-biennial oscillation affect the boreal winter tropospheric circulation in cmip5/6 models? *Journal of Climate*, 33(20):8975–8996, 2020.

N. Rayner, D. E. Parker, E. Horton, C. Folland, L. Alexander, D. Rowell, E. Kent, and A. Kaplan. Global analyses of sea surface temperature, sea ice, and night marine air temperature since the late nineteenth century. *Journal of Geophysical Research: Atmospheres*, 108(D14), 2003.

T. Reichler, P. J. Kushner, and L. M. Polvani. The coupled stratosphere–troposphere response to impulsive forcing from the troposphere. *Journal of the Atmospheric Sciences*, 62(9):3337–3352, 2005. doi: 10.1175/JAS3527.1.

R. Roehrig, I. Beau, D. Saint-Martin, A. Alias, B. Decharme, J.-F. Guérémy, A. Voldoire, A. Y. Abdel-Lathif, E. Bazile, S. Belamari, S. Blein, D. Bouniol, Y. Bouteloup, J. Cattiaux, F. Chauvin, M. Chevallier, J. Colin, H. Douville, P. Marquet, M. Michou, P. Nabat, T. Oudar, P. Peyrillé, J.-M. Piriou, D. Salas y Mélia, R. Séférian, and S. Sénési. The cnrm global atmosphere model arpege-climat 6.3: Description and evaluation. *Journal of Advances in Modeling Earth Systems*, 12(7):e2020MS002075, 2020. doi: https://doi.org/10.1029/2020MS002075.

P. Ruggieri, R. Buizza, and G. Visconti. On the link between barents-kara sea ice variability and european blocking. *Journal of Geophysical Research: Atmospheres*, 121(10):5664–5679, 2016. ISSN 2169-8996. doi: 10.1002/2015JD024021. URL `http://dx.doi.org/10.1002/2015JD024021`. 2015JD024021.

P. Ruggieri, F. Kucharski, R. Buizza, and M. H. P. Ambaum. The transient atmospheric response to a reduction of sea-ice cover in the barents and kara seas. *Quarterly Journal of the Royal Meteorological Society*, 143 (704):1632–1640, 2017. ISSN 1477-870X. doi: 10.1002/qj.3034. URL `http://dx.doi.org/10.1002/qj.3034`.

P. Ruggieri, F. Kucharski, and L. Novak. The response of the midlatitude jet to regional polar heating in a simple storm-track model. *Journal of Climate*, 32 (10):2869–2885, 2019.

P. Ruggieri, A. Bellucci, D. Nicolì, P. J. Athanasiadis, S. Gualdi, C. Cassou, F. Castruccio, G. Danabasoglu, P. Davini, N. Dunstone, et al. Atlantic multidecadal variability and north atlantic jet: A multimodel view from the decadal climate prediction project. *Journal of Climate*, 34(1):347–360, 2021.

Y. Ruprich-Robert, R. Msadek, F. Castruccio, S. Yeager, T. Delworth, and G. Danabasoglu. Assessing the climate impacts of the observed atlantic multidecadal variability using the gfdl cm2.1 and ncar cesm1 global coupled models. *Journal of Climate*, 30(8):2785–2810, 2017. doi: 10.1175/JCLI-D-16-0127.1.

K. Saito and J. Cohen. The potential role of snow cover in forcing interannual variability of the major northern hemisphere mode. *Geophysical Research Letters*, 30(6), 2003. doi: https://doi.org/10.1029/2002GL016341.

A. Sanna, A. Borrelli, P. Athanasiadis, S. Materia, A. Storto, A. Navarra, S. Tibaldi, S. Gualdi, et al. Cmcc-sps3: the cmcc seasonal prediction system 3. *CMCC Research Paper*, (RP0285), 2016.

K. L. Smith, C. G. Fletcher, and P. J. Kushner. The role of linear interference in the annular mode response to extratropical surface forcing. *Journal of Climate*, 23(22):6036–6050, 2010. doi: 10.1175/2010JCLI3606.1.

L. Song and R. Wu. Intraseasonal snow cover variations over western siberia and associated atmospheric processes. *Journal of Geophysical Research: Atmo-*

spheres, 124(16):8994–9010, 2019. doi: 10.1029/2019JD030479.

A. Wald and J. Wolfowitz. On a test whether two samples are from the same population. *The Annals of Mathematical Statistics*, 11(2):147–162, 1940.

D. Walters, I. Boutle, M. Brooks, T. Melvin, R. Stratton, S. Vosper, H. Wells, K. Williams, N. Wood, T. Allen, et al. The met office unified model global atmosphere 6.0/6.1 and jules global land 6.0/6.1 configurations. *Geoscientific Model Development*, 10(4):1487–1520, 2017.

J. Wang, H. Kim, D. Kim, S. A. Henderson, C. Stan, and E. D. Maloney. Mjo teleconnections over the pna region in climate models. part i: Performance-and process-based skill metrics. *Journal of Climate*, 33(3):1051–1067, 2020.

L. Wang, M. Ting, and P. Kushner. A robust empirical seasonal prediction of winter nao and surface climate. *Scientific reports*, 7(1):1–9, 2017.

Table 1 Description of the seasonal prediction systems used in this study. Columns indicate, from left to right, the modelling centre and the system version, the resolution, the size of the ensemble the method used to initialize snow cover, the land model and a reference for the land model. The JRA55 reanalysis is documented in Kobayashi et al. [2015]. The ERA-Interim (ERA-I) reanalysis is documented in Dee et al. [2011]. Here a forced run is an offline land-only run forced with meteorological forcing.

System	Resolution	Ens. Size	Snow I.C.	Land model	Ref.
CMCC 3	1×1 L46	40	Forced run	CLM4.5	Oleson et al. [2013]
MF 6	TL359 L91	25	ERA-I	SURFEX v8.1	Le Moigne et al. [2009]
ECMWF 5	T_{CO}319 L91	25	Forced run	IFS 43r1	Johnson et al. [2019]
DWD 2	T127 L95	30	Indirect	JSBACH	Brovkin et al. [2009]
UKMO 13	N216 L95	21	JRA55	JULES GL 6	Walters et al. [2017]

Table 2 Projection onto the model AO pattern of the response (SNOW minus CONTROL) in idealised simulations with the CMCC-AGMC model and the MF-AGCM model.

Month	CMCC	MF
OCT	-0.17	0.23
NOV	-0.33	0.53
DEC	-1.22	-0.10
JAN	-0.05	-0.71
FEB	0.29	-0.23

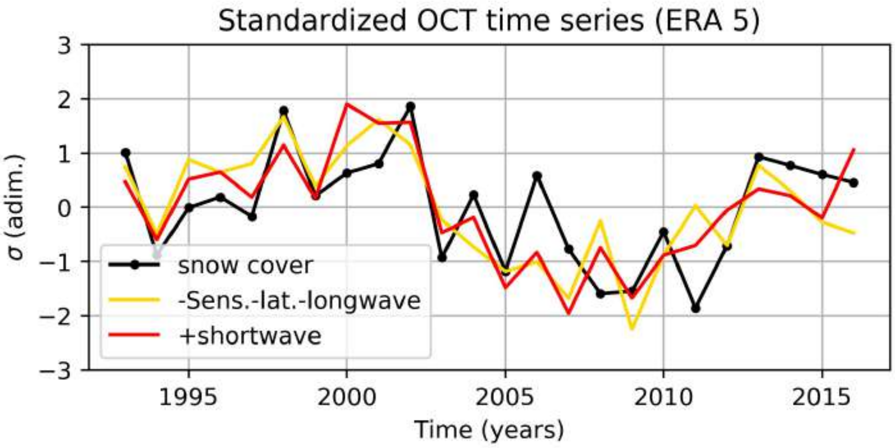

Fig. 1 Standardized time series of October snow covered area fraction (snow cover, black line) and October surface heat fluxes over Eurasia (42.5°N-72.5°N 40°E-180°E, only grid point entirely over land are used) derived from ERA5-Land in the period covered by C3S seasonal forecast. Fluxes are defined as positive when upward. The red line indicates the shortwave flux, while the yellow line indicates the sum of sensible, latent and longwave flux with a minus sign.

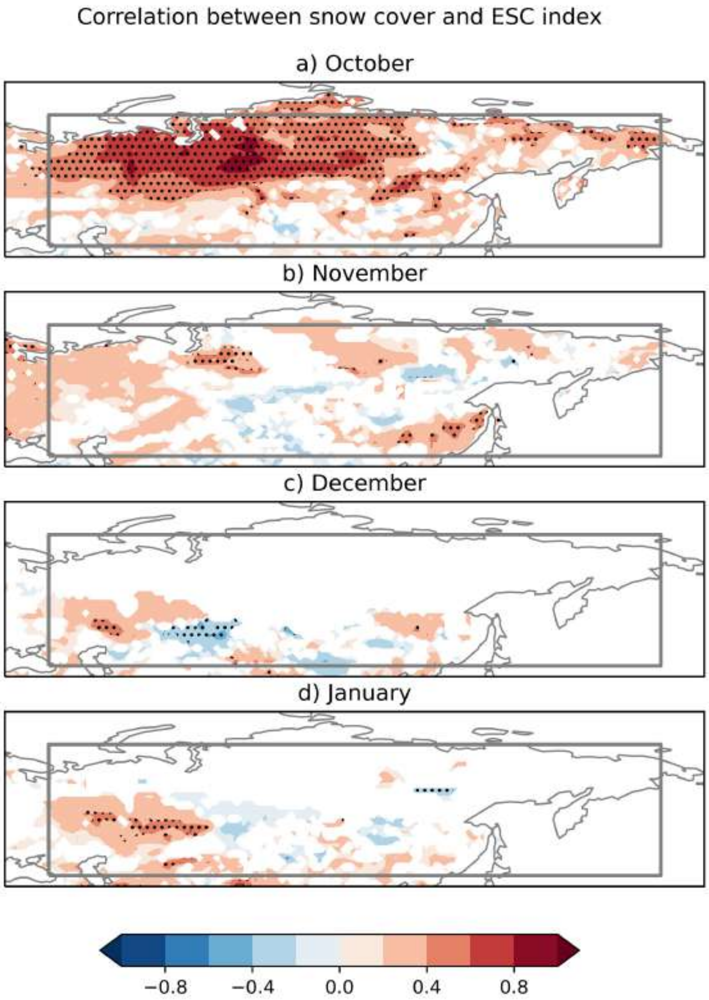

Fig. 2 Correlation between monthly mean snow cover in ERA5-Land and the October ESC index. Values between -.1 and .1 are not displayed. Grey rectangles encompass the area used to compute averaged quantities displayed in Fig. 1.

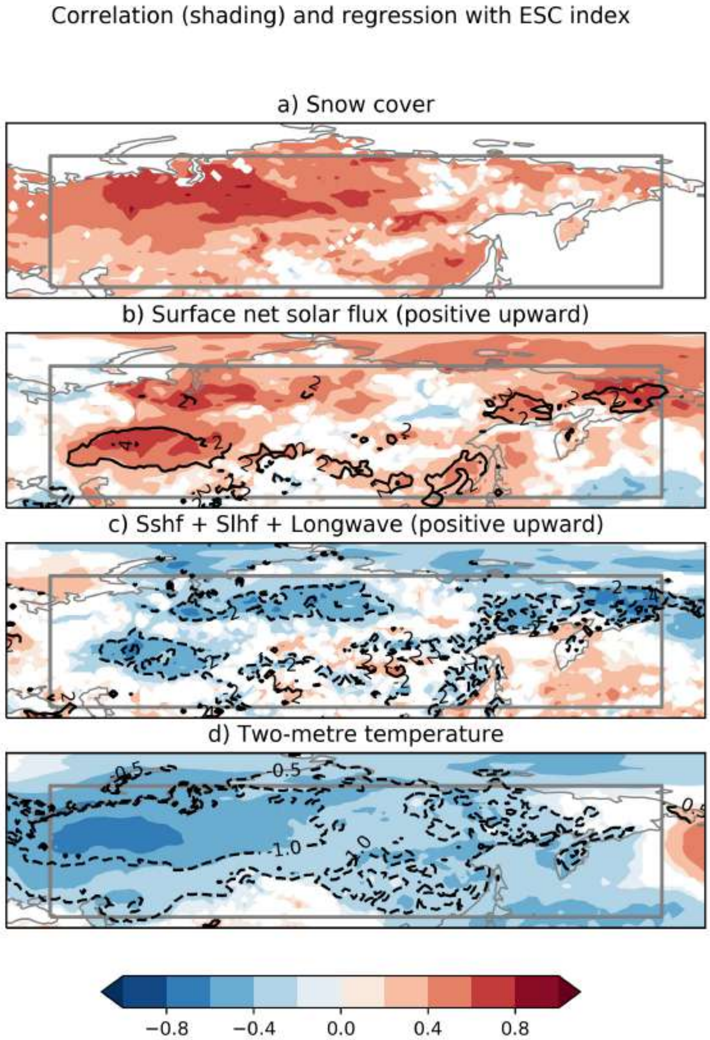

Fig. 3 Correlation (shading) and regression (contours) of October-November mean ERA5-land snow cover, and ERA5 surface fluxes and two-metre temperature (T2m) and the October ESC index in ERA5-Land, shown in Fig. 1 with a black line. All fluxes are defined as positive when upward. a) Correlation of snow cover. b) Correlation and regression of the sum of sensible heat flux, latent heat flux and net longwave flux. c) as in b) but for the net shortwave flux and d) for two-metre temperature. Units for the regression are $Wm^{-}2$ in b) and c) and K in d). Values between -.1 and .1 are not displayed.

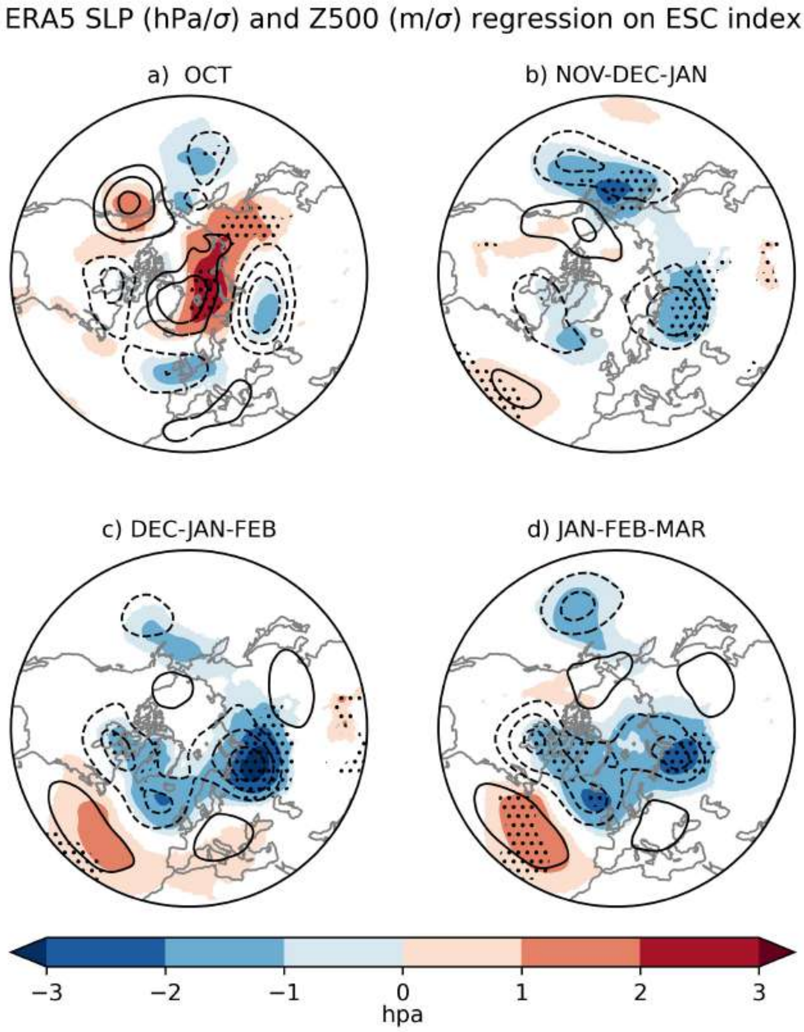

Fig. 4 ERA5 regression coefficients on the October ESC index of Z500 (contours drawn at ± 10, 20 and 30 m) and SLP (shadings, hPa) averaged in a) October, b) OND, c) NDJ and d) DJF. Stippling indicates region where the regression is statistically significant at 95% confidence level. Values between -.5 and .5 hPa are not displayed.

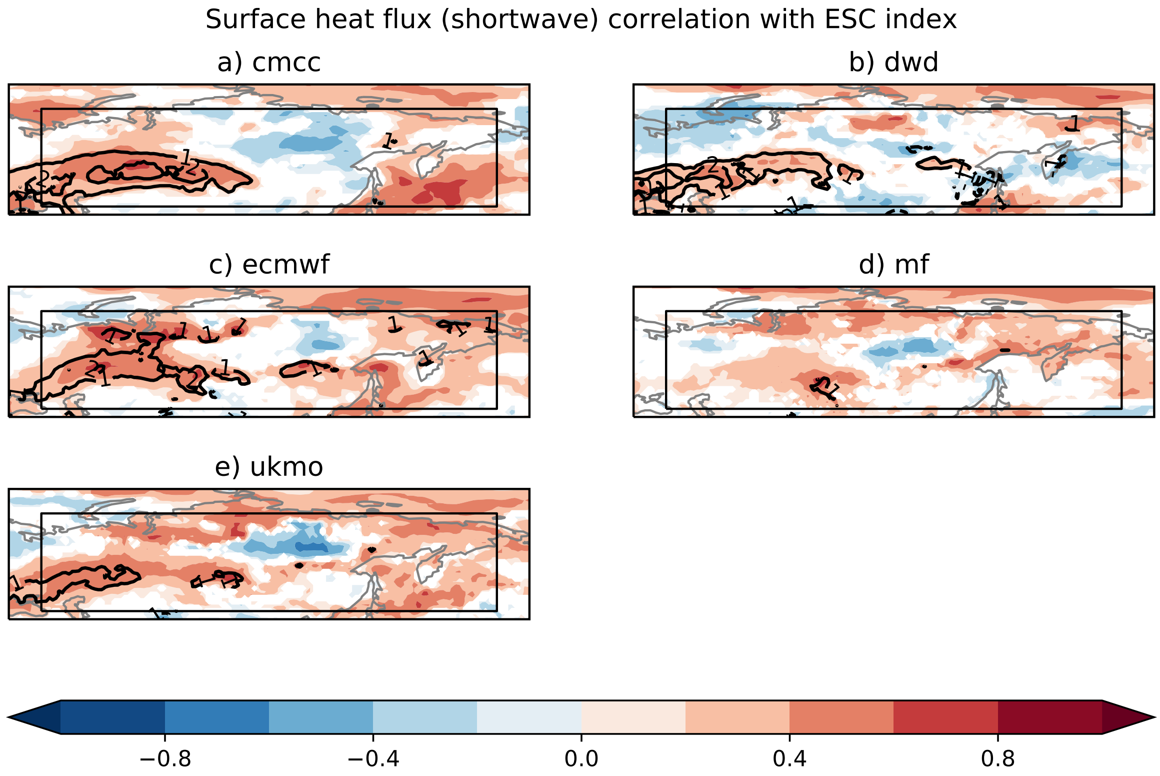

Fig. 5 Correlation (shadings) and regression (contours, drawn at ± 1, 2 Wm^{-2}) between the flux of shortwave radiation and the October ESC index in ERA5-Land for 5 seasonal hindcasts. Values between -.1 and .1 are not displayed.

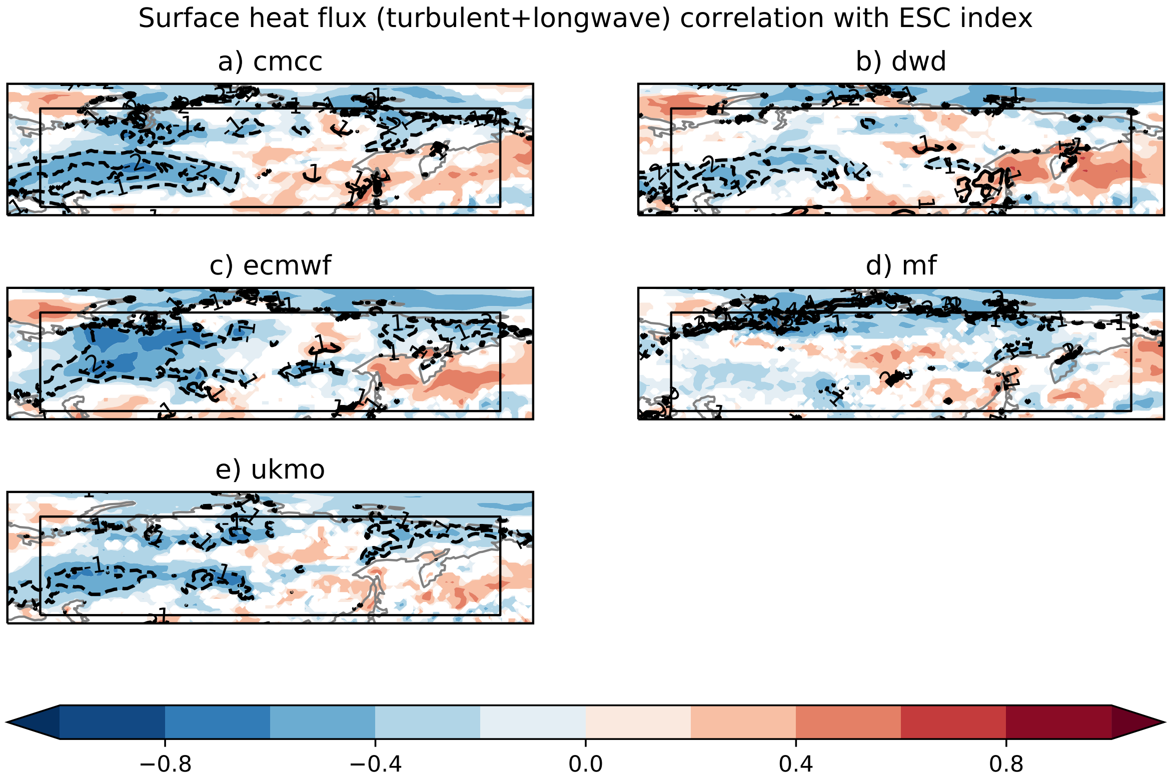

Fig. 6 As in Fig. 5 but for the sum of sensible heat, latent heat and thermal radiation.

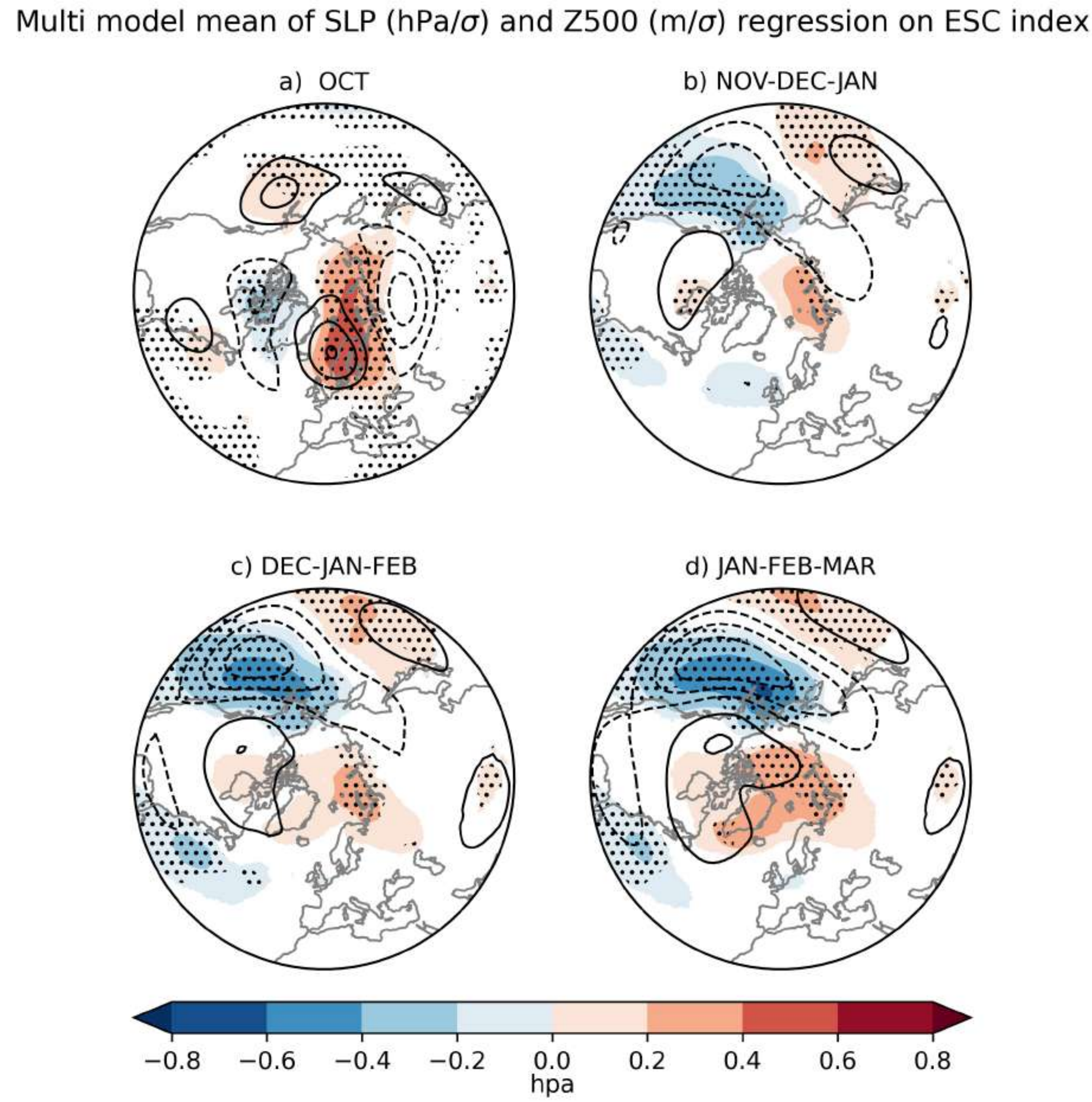

Fig. 7 Multi-model (5 seasonal hindcasts) mean of regression coefficients on the October ESC index in ERA5-Land of Z500 (contours drawn ± 6, 12 and 18 m in a) and at ± 2, 4 and 6 m in b),c) d)) and SLP (shadings, hPa) averaged over a) October, b) NDJ, c) DJF and d) JFM. Stippling indicates region where all models have the same sign for SLP. SLP values between -.1 and .1 hPa are not displayed and SLP values in a) have been scaled by a factor of 1/3.

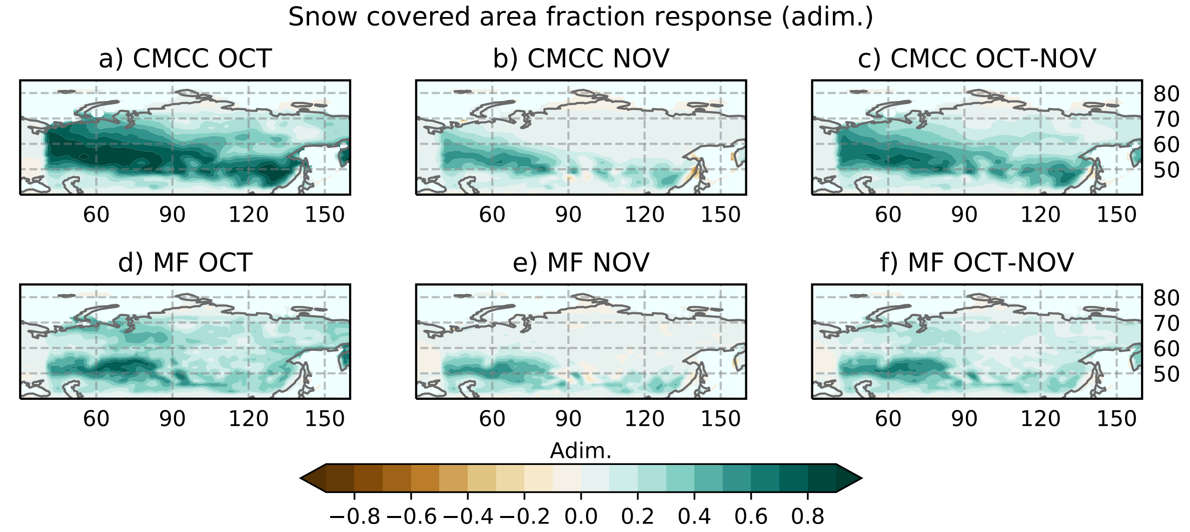

Fig. 8 Response of the snow cover in the idealized AGCM experiments in October (a, d), November (b, e) and their average (c, f) for the CMCC-AGCM model (top row) and the MF-AGCM model (bottom row).

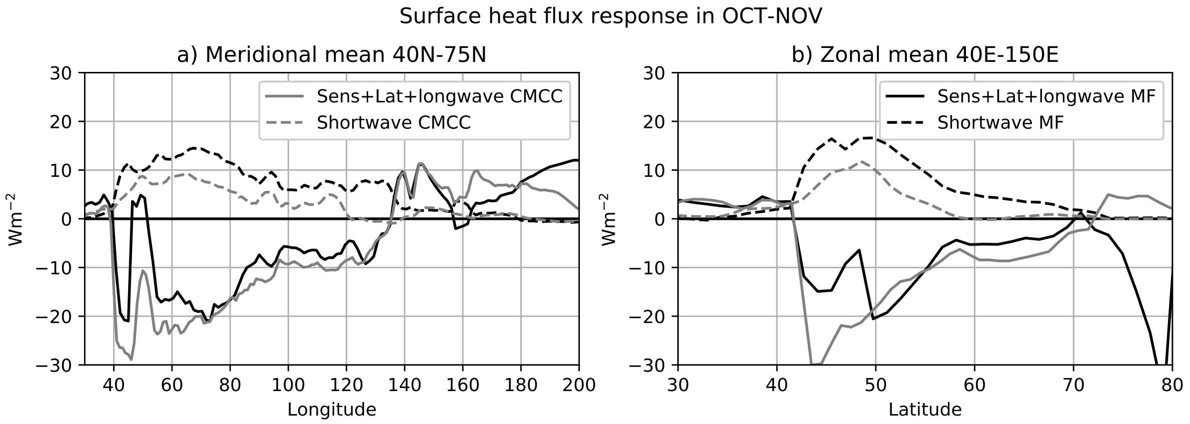

Fig. 9 Surface heat flux response in October and November in the idealised experiments with the CMCC-AGCM (grey lines) and MF-AGCM (black lines) model. The dashed lines are used for shortwave radiation and the solid lines for the sum of longwave, sensible and latent heat fluxes. In panel a) fluxes are averaged meridionally (weighted by the area) between 40 and 70 °N, in b) they are averaged zonally between 40 and 150 °E.

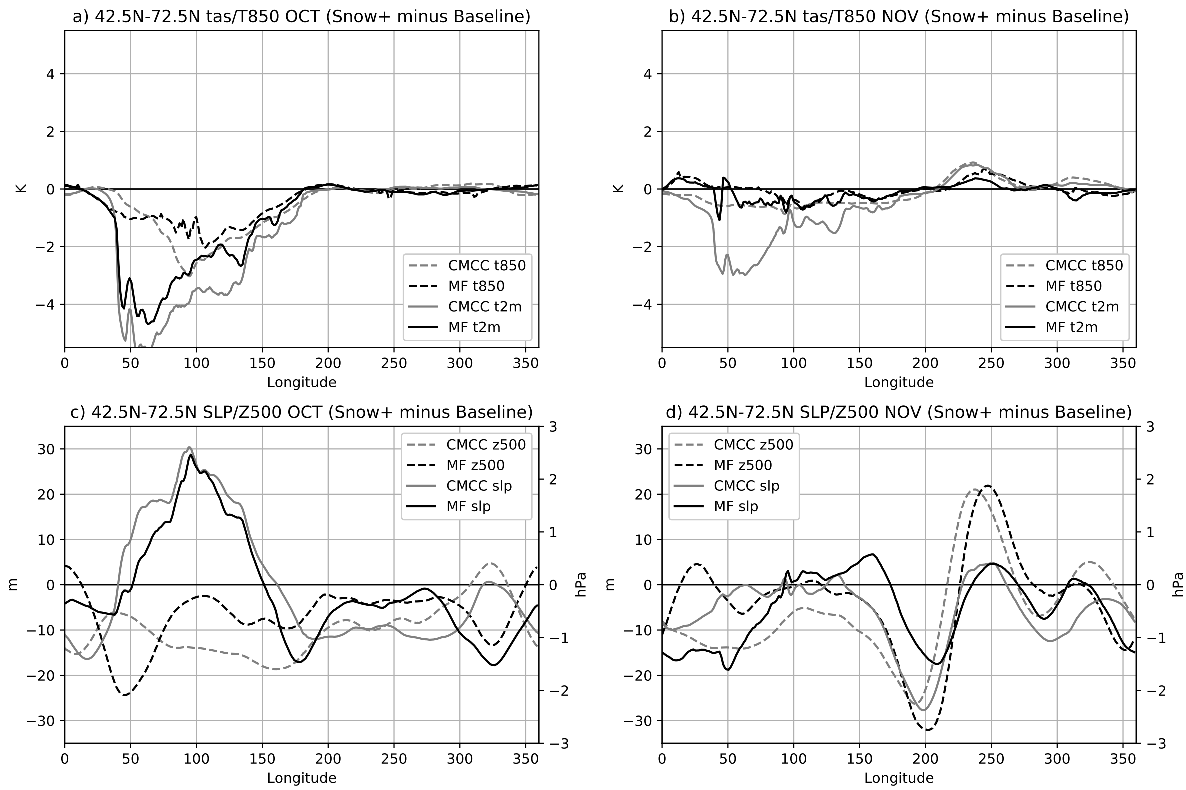

Fig. 10 Meridional mean (area-weighted) between 42.5N and 72.5N of T2m (solid lines, K) and T850 (dashed lines, K) in a) OCT and b) NOV for the idealized AGCM experiments with the CMCC-AGCM model (grey lines) and the MF-AGCM (black lines) model. c) and d) As in a) and b) but for SLP (solid lines, hPa) and Z500 (dashed lines, m).

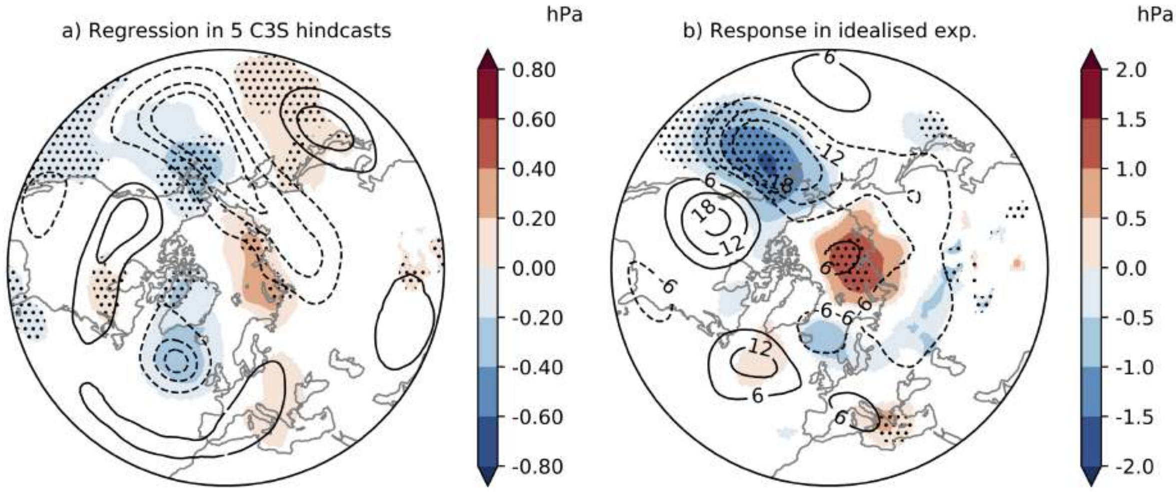

Fig. 11 November-December Atmospheric response to October snow cover increase inferred from C3S hindcasts (a) and idealised simulations (b). In a), the multi-model mean regression coefficient is shown for Z500 (contours drawn at $\pm 1.5, 2.25, 3, 3.75$ m) and SLP (shadings). Stippling indicates regions where all models agree on the sign of the regression. In b), the response to snow cover defined two-model mean of the ensemble mean difference (SNOW-CONTROL). As in a), Z500 is shown by contours drawn at $\pm 6, 12, 18$ and SLP is shown with shadings. Stippling indicates regions where the two models have the same sign of the response.

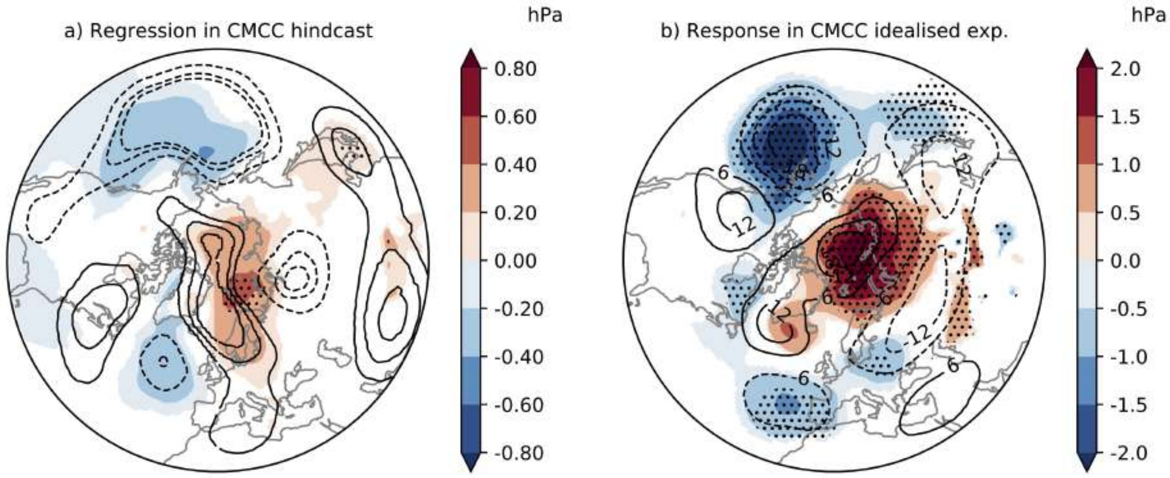

Fig. 12 As in Fig. 11 but using the CMCC-AGCM model instead of the multi-model mean. Stippling indicates statistically significant values at 95% confidence level.

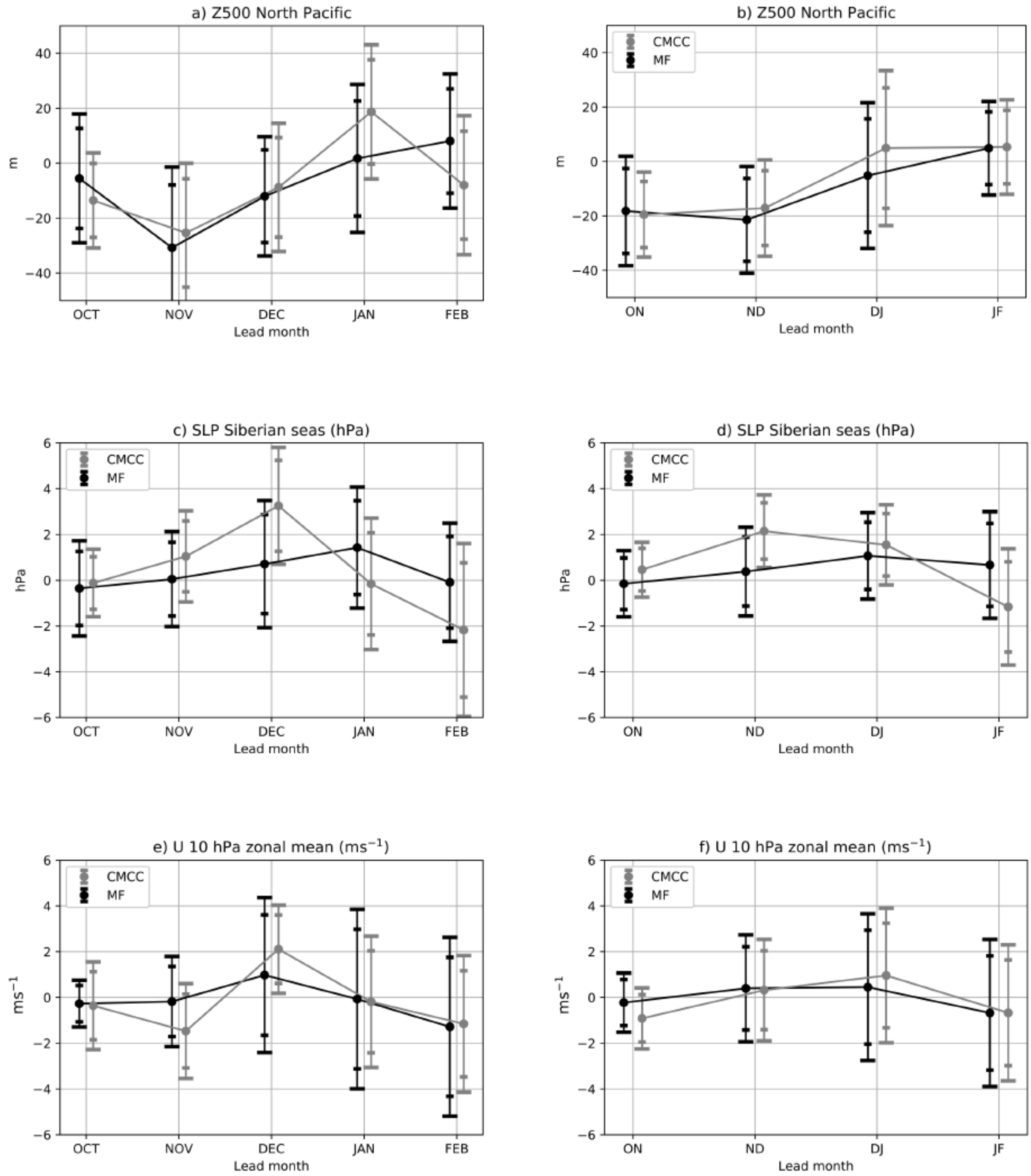

Fig. 13 Circulation response in the idealised simulations with the CMCC-AGCM (grey lines) and MF-AGCM (black lines) models. Bars indicate the confidence interval at 80% and 90% confidence level. Values are averaged monthly in the left column and bimonthly in the right column. a) and b) show Z500 averaged in the Northern extratropical Pacific (45-65 °N, 180-210 °E). c) and d) show SLP averaged in the Siberian sector of the Arctic ocean (75-90 °N, 55-150 °E, over the East Siberian sea and the Laptev sea). e) and f) zonal mean of the zonal wind at 10 hPa between 55 and 65 °N.

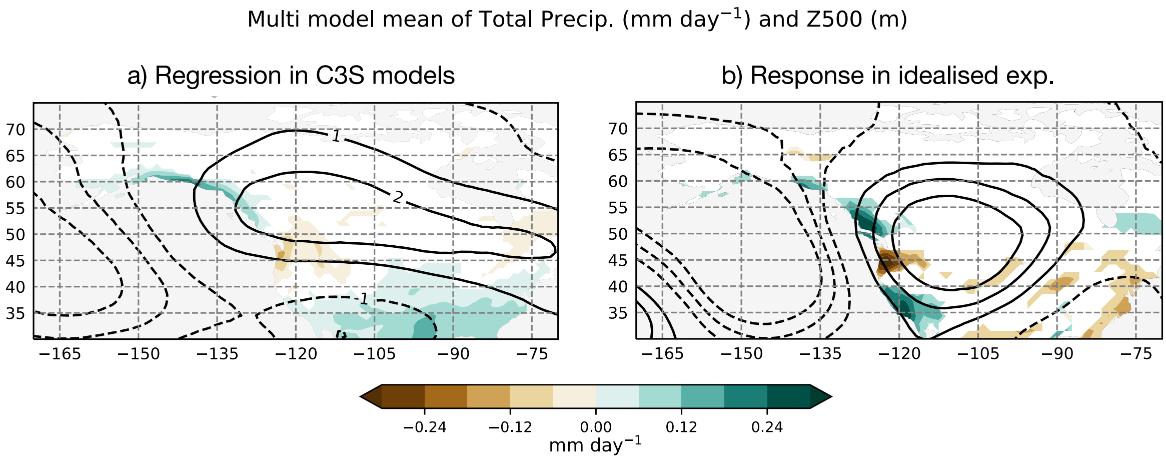

Fig. 14 a) Multi-model mean regression coefficient with the ESC index in ERA5-Land of Z500 (contours, drawn every 1 m, zero line omitted) and precipitation (shadings, mm day^{-1}) in seasonal hindcasts. b) Multi-model mean response to snow cover increase in idealised simulation. Contours of Z500 are drawn every 6 m (zero line omitted) and shadings are used for precipitation.